Homogeneous and inhomogeneous broadening in single perovskite nanocrystals investigated by micro-photoluminescence

Hamid Pashaei Adl [a], Setatira Gorji [a], Guillermo Muñoz-Matutano [a,**], Raúl I. Sánchez-Alarcón [a], Rafael Abargues [a], Andrés F. Gualdrón-Reyes [b,c], Iván Mora-Seró [b], Juan P. Martínez-Pastor [a,*]

[a] *Instituto de Ciencia de Materiales (ICMUV), Universidad de Valencia, C/ Catedrático José Beltrán, 2, E-46980, Paterna, Spain*
[b] *Institute of Advanced Materials (INAM), Universitat Jaume I (UJI), Avenida de Vicent Sos Baynat, S/n 12071, Castellón, de La Plana, Spain*
[c] *Facultad de Ciencias, Instituto de Ciencias Químicas, Isla Teja, Universidad Austral de Chile, 5090000, Valdivia, Chile*

ARTICLE INFO

ABSTRACT

Metal halides with perovskite crystalline structure have given rise to efficient optoelectronic and photonic devices. In the present work, we have studied the light emission properties of single $CsPbBr_3$ and $CsPbI_3$ semiconductor perovskite nanocrystals (PNCs), as the basis for a statistical analysis of micro-photoluminescence (micro-PL) spectra measured on tens of them. At room temperature, the linewidth extracted from PL spectra acquired in dense films of these nanocrystals is not very different from that of micro-PL measured in single nanocrystals. This means that the homogeneous linewidth due to exciton-phonon interaction is comparable or larger than the inhomogeneous effect associated to the micro-PL peak energy dispersion due to the nanocrystal size distribution defined by the chemical synthesis of the PNCs. Contrarily, we observe very narrow micro-PL lines in $CsPbBr_3$ and $CsPbI_3$ PNCs at 4 K, in the range of 1–5 meV and 0.1–0.5 meV, respectively, because they are limited by spectral diffusion. Aging of PNCs under ambient conditions has been also studied by micro-PL and a clear reduction of their nanocube edge size in the order of the nm/day is deduced.

1. Introduction

Semiconductor nanocrystals are crystalline structures with size at the nanoscale (1–100 nm), which possess electronic and optical properties according to their semiconductor condition (bandgap energy, energy band dispersion, absorption coefficient, exciton lifetime, etc.), in addition to a possible quantum confinement effect of carriers/excitons due to size reduction. Particularly, if they proceed from direct bandgap semiconductors, efficient light emitters devices [1], and even quantum light emitters at room temperature (RT) [2], can be developed, among other applications. The structure of perovskite nanocrystals (PNCs) are compounds with general formula ABX_3, being A an inorganic or organic bulky cation, B a metal cation such as Pb^{2+} or Sn^{2+} and X the halide anion, in the case of metal halide perovskites. Taking into account the chemical synthesis of these perovskite materials [3], a wide range of possibilities can be achieved in terms of their crystalline structure: different phases (cubic, orthorhombic, …) [4], morphology (nano-platelets [5,6], nanowires [7] and nanocubes [8]) and chemical

composition [6,9,10]. The optical properties of metal halide perovskites are susceptible to all these modifications, being the basis of their application in various optoelectronic devices, as the case of electroluminescent diodes [11,12], photodetectors [13] and solar cells [14–17], whose progress has been spectacular in the recent ten years, as the 25.5% of record efficiency under sun illumination [18]. A remarkable point of the $CsPbX_3$ PNCs is the tuning of their band gap, and consequently of their light emission spectrum, by modifying the composition of the halide anion (X): their peak wavelength is observed at around 400 nm (near UV), 510 nm (green) and 680 nm (deep red) for X = Cl, Br and I, respectively, in addition to the $Cl_xBr_yI_{1-x-y}$ combinations with $0 \leq x, y \leq 1$ [9]. When talking about the photoluminescence (PL) in PNCs and, in general, in any bulk or low-dimensional semiconductor, it is necessary to speak about their efficiency or PL quantum yield (PLQY), which refers to the number of photons emitted with respect to those absorbed by the material, or the ratio between radiative to the total rate, radiative and non-radiative. Specifically, in $CsPbX_3$ PNCs, the PLQY is greater than 40% [19], although with the appropriate treatment, values close to

100% [20] can be achieved in colloidal suspensions for X = Br [21], X = I [22] and X = Cl [23]. Moreover, it is noteworthy to mention that light emission of these PNCs is characterized by high color purity, with PL Full Width at Half Maximum (FWHM) as low as 20 nm for $CsPbBr_3$ (green emission) [21] and less than 15 nm for those of $CsPbCl_3$ (emission in blue-violet) [23]. Due to aforementioned outstanding features of $CsPbX_3$ PNCs, they can be potential candidates not only in photonic applications [24–27], but also in quantum light technologies, as a single photon sources [28–30].

In this work we have analyzed single nanocrystals by means of micro-PL spectroscopy. We have deduced an average peak energy for the excitonic optical transitions of 2.414 and 1.830 eV for PNCs of $CsPbBr_3$ and $CsPbI_3$, respectively, in freshly prepared samples. However, a blue shift of these energies is clearly observed when PL measurements are made one or more days after sample preparation. We attribute this effect to an effective decrease of the (individual) nanocrystal size due to the interaction with ambient humidity. The measured dispersion in the excitonic transition energies (in fresh samples) can be accounted for by a simple cubic quantum dot model with finite potential barriers applied to the size distribution of PNCs. On the basis of this model applied to the data sets of $CsPbBr_3$ PNCs, we are able to deduce size reductions for aging under ambient conditions in the order of 1.5 and 0.8 nm/day. We have also demonstrated that the FWHM of the PL measured in a dense layer of PNCs is not far from the average value of this magnitude found from micro-PL measured in single nanocrystals (i.e., their homogeneous linewidth), around 68 meV, which is limited by exciton-phonon interaction at RT. This is explained because PNCs are subject to weak

quantum size confinement and size dispersion (even if important, 0.8–2 nm depending on the synthesis method) is not determinant to define a noticeable inhomogeneous contribution to the PL FWHM and hence dominates the exciton homogenous linewidth. We also did similar investigation on single PNCs by micro-PL characterization at low temperatures (4 K), where the homogeneous linewidth of excitonic optical transitions is much smaller than the inhomogeneous value associated to the size dispersion of PNCs. The average energy for the excitonic optical transitions were found at 2.325 and 1.830 eV, whereas their excitonic homogenous linewidths were in the range of 1–5 meV and 0.1–0.5 meV, for $CsPbBr_3$ and $CsPbI_3$ PNCs, respectively, whose difference is ascribed to another broadening effect: spectral diffusion, dominating at low temperatures.

2. Results

Details on synthesis of $CsPbBr_3$ and $CsPbI_3$ PNCs, preparation of samples with dispersed single nanocrystals and experimental micro-PL setups at RT and 4 K are given in section S1 of the Supplementary Info. Fig. 1 shows three micro-PL images (top panels) and spectra (bottom panels) at RT in three different areas of the sample containing $CsPbBr_3$ PNCs. In these images each single PNC is distinguished as green light circles. The micro-PL spectra at the bottom panels correspond to the four bright green circles selected in the two top images, the blue dashed circle in the first image schematically shows our collection spot size. The black continuous lines in plots of Fig. 1 (bottom panels) correspond to the best fittings to a Lorentzian profile. These fits are the
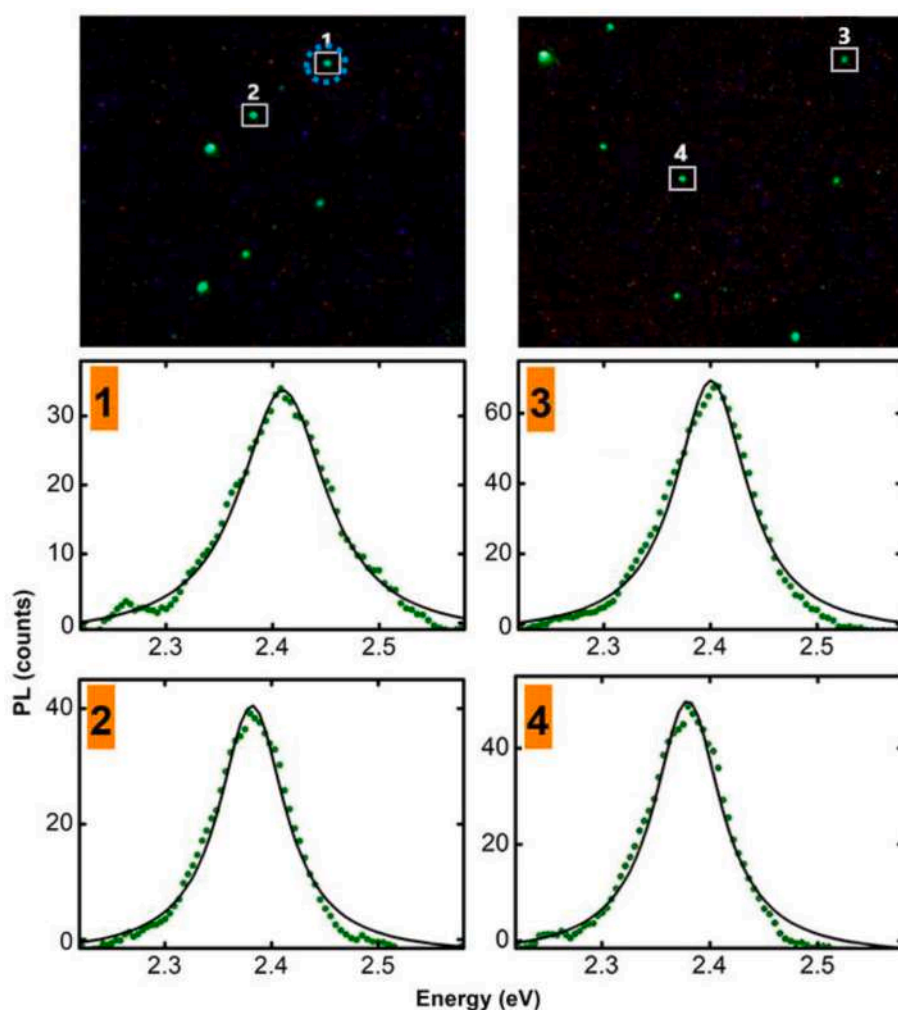

Fig. 1. (top panels) Micro-PL images at room temperature captured with the C-MOS camera (2s exposure) from two different regions of the sample containing $CsPbBr_3$ PNCs emitting at green wavelengths (green circles that have been boxed and marked with numbers 1 to 4). These circles of green light have a repetition image beneath them, due to the second surface of the quartz plate (1 mm thick) that is being used as a signal beam splitter. The different single-color points observed in the images correspond to individual pixels of the camera due to background noise. (bottom panels) Experimental micro-PL spectra (green dotted lines) corresponding to the $CsPbBr_3$ PNCs selected in top panels. Continuous lines stand for a Lorentzian shape fitting, as explained in the text.

basis of our statistical study in CsPbBr$_3$ PNCs. The micro-PL spectra in freshly prepared samples with PNCs of the first synthesis (see morphology and size distribution in top panels of Figure S1 in Supp. Info.) are centered typically at around 2.4 eV (or 516 nm) and have a FWHM from 70 to 100 meV (15–21 nm), which accounts for the size distribution of these PNCs. These values are consistent with those obtained in Refs. [9,31] for films of CsPbBr$_3$ PNCs with similar size. It is worth mentioning the case of some brighter green spots in Fig. 1, where the PL intensity is higher (may be more than one PNC is emitting simultaneously at this spatial location), but with very similar shape and FWHM.

For calibration purposes, we have also measured PL spectra in a sample containing a continuous uniform layer of CsPbBr$_3$ PNCs (Figure S4). As can be seen in the image captured by the CCD camera (see inset in Figure S4), the PL of discrete nanocrystals cannot be distinguished anymore. In spite of this high-density ensemble of PNCs, its PL spectrum is not very different from those measured in single nanocrystals (Fig. 1). Even a Lorentzian fit (black continuous curve in Figure S4) is reasonably good for the continuous layer, obtaining a peak energy of 2.422 eV (512 nm) and a FWHM = 105 meV (22 nm). Possibly, the PL peak energy dispersion (inhomogeneous broadening) observed in single PNCs would be smaller than their homogeneous linewidth at RT, as will be discussed below.

Similar findings are observed in single CsPbI$_3$ PNCs at RT (see morphology and size distribution in Figure S2 of Supp. Info.). Fig. 2a shows the emission from several single nanocrystals (reddish circles in the image) captured by the microscope camera, whereas a representative micro-PL spectrum of one of them is shown in Fig. 2b (red data symbols). Again, this spectrum can be nicely fitted by a Lorentzian line shape (solid black curve in Fig. 2b). The micro-PL peak energy is found at around 1.83 eV (680 nm) with a FWHM of around 100 meV (about 40 nm), also very similar to values referred in literature for CsPbI$_3$ PNCs of similar size [32]. In these samples we observe that micro-PL intensity decreases rapidly with time under ambient conditions, the more the greater the power of the excitation laser. In the case of samples with CsPbBr$_3$ PNCs this phenomenology was not observed until a relatively high excitation laser power, a fact attributed to the lower black phase stability for these PNCs [33], which makes more difficult their statistical study.

In a certain percentage of single PNCs in freshly prepared samples, we observed the phenomenon of intensity intermittency or blinking. Figures S5 and S6 of the Supp. Info. shows respectively, a sequence of micro-PL images in which the off-on-off sequence is observed during 40 s in one of the single PNCs. This phenomenon is an effect clearly associated to isolated nanocrystals, as also observed in semiconductor quantum dots and in different types of molecules.

Fig. 3a–c demonstrate how micro-PL spectra of CsPbBr$_3$ (green lines) and CsPbI$_3$ (brown lines) PNCs at 4 K, respectively, exhibit very narrow lines that cover the energy range of the inhomogeneous PL spectra of the corresponding high-density samples (black curves). In fact, the frequency histograms for micro-PL peak energies measured in 80 and 30 single PNCs of CsPbBr$_3$ and CsPbI$_3$ clearly overlap with the PL spectra of their corresponding high-density films, as shown in Fig. 3b–d. Therefore, the observed PL inhomogeneity in the high-density samples would proceed from the observed micro-PL peak energy dispersion at 4 K, which is attributed here to the nanocrystal size distribution in our PNCs (Figures S1 and S2), as we will further demonstrate below by exciton energy calculations Figure S1. It is also worth noting that micro-PL spectra of individual CsPbI$_3$ PNCs are much narrower than the CsPbBr$_3$ ones at 4 K, but they are very similar at RT (see Figures S7-S8 in Supp. Info. for direct comparison). Quantitatively, the linewidths of CsPbI$_3$ PNCs are mostly below 0.5 meV, whereas the CsPbBr$_3$ emission can reach values as high as 5 meV (see the frequency histogram in Figure S9 of the Supp. Info.).

3. Discussion

The emission energy of a single PNC will vary with the nanocube edge size and hence the observed size distributions (Figures S1 and S2 for CsPbBr$_3$ and CsPbI$_3$, respectively) would be the origin of the observed micro-PL peak energy dispersion (Fig. 3). Moreover, such dispersion is significantly smaller than the homogenous linewidth of micro-PL spectra at RT, as it is clearly demonstrated for CsPbBr$_3$ and CsPbI$_3$ PNCs in Fig. 4a–c. Indeed, for 40 single CsPbBr$_3$ PNCs measured immediately after the sample preparation, the dispersion in the micro-PL peak energies turns out to be in the order of 50 meV (frequency histogram in Fig. 4a), lower than the homogeneous linewidth of a representative PNC in this sample (green shaded curve in Fig. 4a), whose Lorentzian linewidth was ≈85 meV and being its average value 94 ± 11 meV. Similarly, the dispersion in the peak energies of the micro-PL lines measured in 20 CsPbI$_3$ PNCs of the fresh sample was smaller than 40 meV (frequency histogram in Fig. 4c), lower than half of the homogeneous linewidth (≈100 meV) extracted from a representative micro-PL spectrum (red-shaded curve in Fig. 4c). The same occurs for PNCs measured the next day after preparation. However, we also observe a clear shift of the micro-PL peak energies towards the blue, an effect that will be discussed below. The fact of a small dispersion of PL peak energies in PNCs as compared to their homogeneous linewidth would have a great impact on developing display devices with high color purity [34].
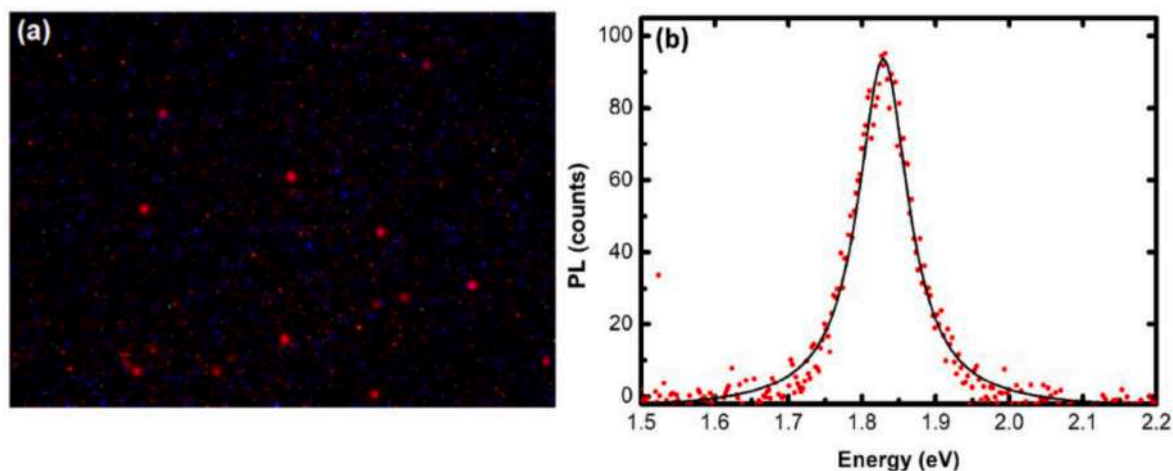

Fig. 2. (a) Typical image captured with the microscope camera, (b) A representative micro-PL spectrum of one of the CsPbI$_3$ PNCs (red dotted curves) in a fresh sample at RT, along with the Lorentzian fit (continuous black curves).
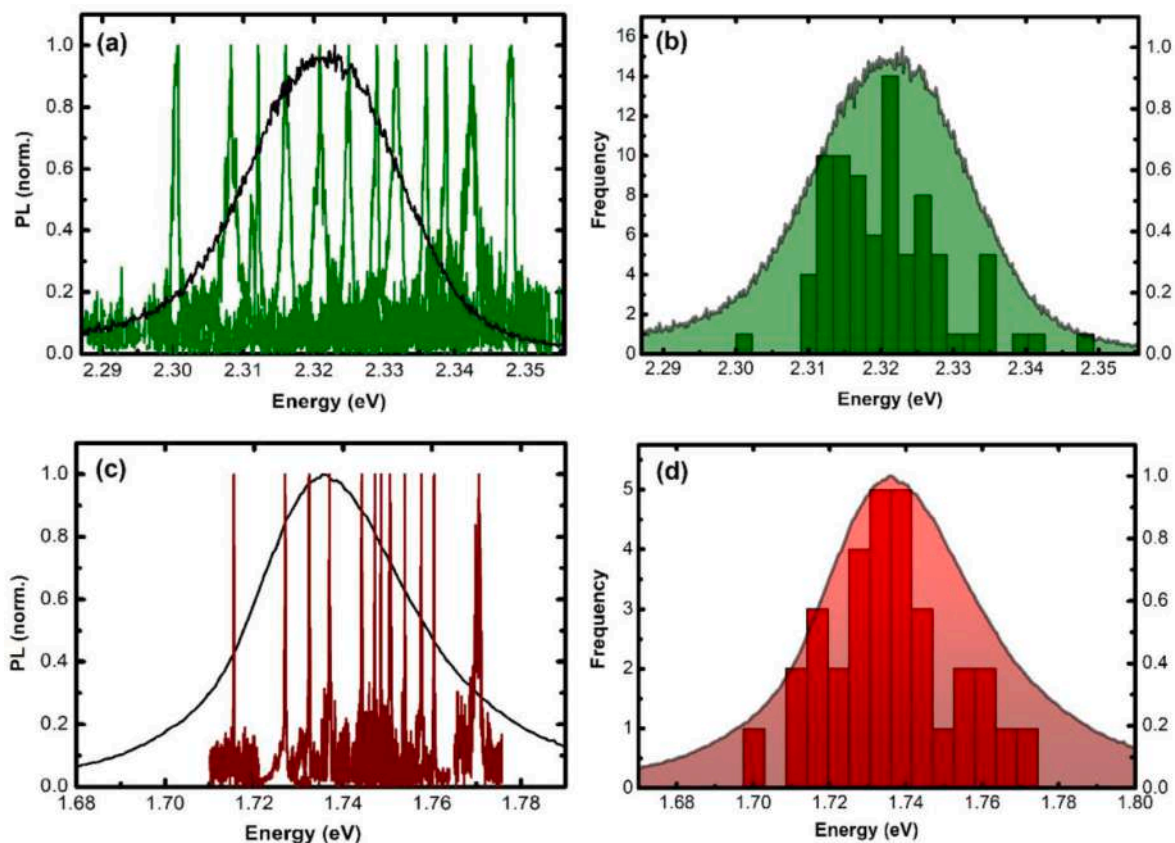
Fig. 3. (a–c) Representative micro-PL spectra at 4 K of CsPbBr$_3$ (green curves) and CsPbI$_3$ (brown curves) PNCs as compared to the PL spectra (black curves) of the corresponding high-density samples. (b–d) Statistics obtained for the micro-PL peak energies in around 80 CsPbBr$_3$ (green histogram) and more than 30 CsPbI$_3$ (red histogram) single PNCs. Green and red shadowed curves in (b–d) are the same reference PL spectra as in (a–c).
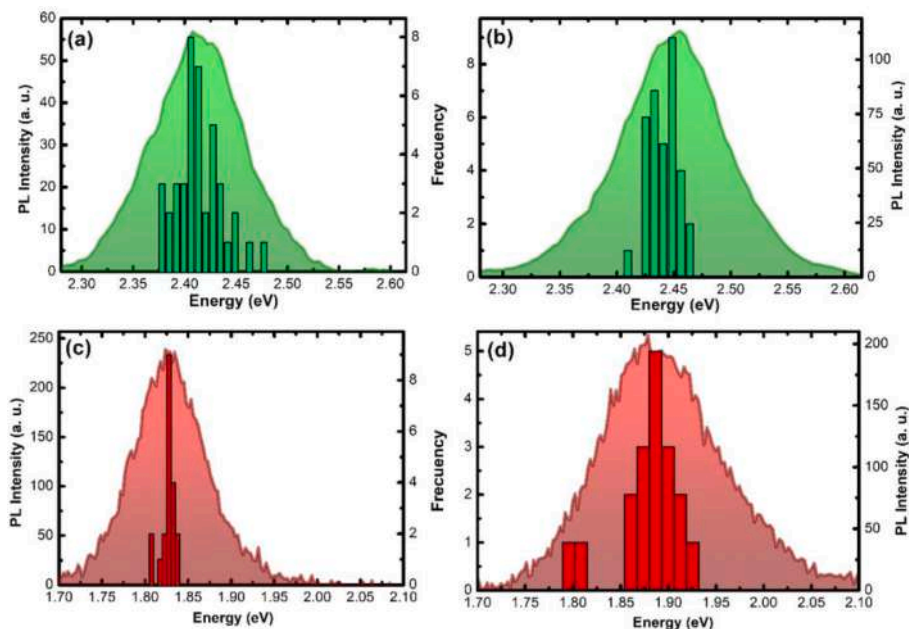

Fig. 4. (a–c) Histograms of peak energies extracted from micro-PL spectra measured at RT in 41 (green color) and 20 (red color) of CsPbBr$_3$ (a) and CsPbI$_3$ (c) PNCs (first synthesis) in fresh samples, respectively. (b–d) idem for the case of 34 and 18 PNCs of the same samples measured next day. In all cases, representative homogeneous micro-PL spectra (similar to those in Figs. 1 and 2) are plotted as green- and red-shaded curves for CsPbBr$_3$ (a–b) and CsPbI$_3$ (c–d).
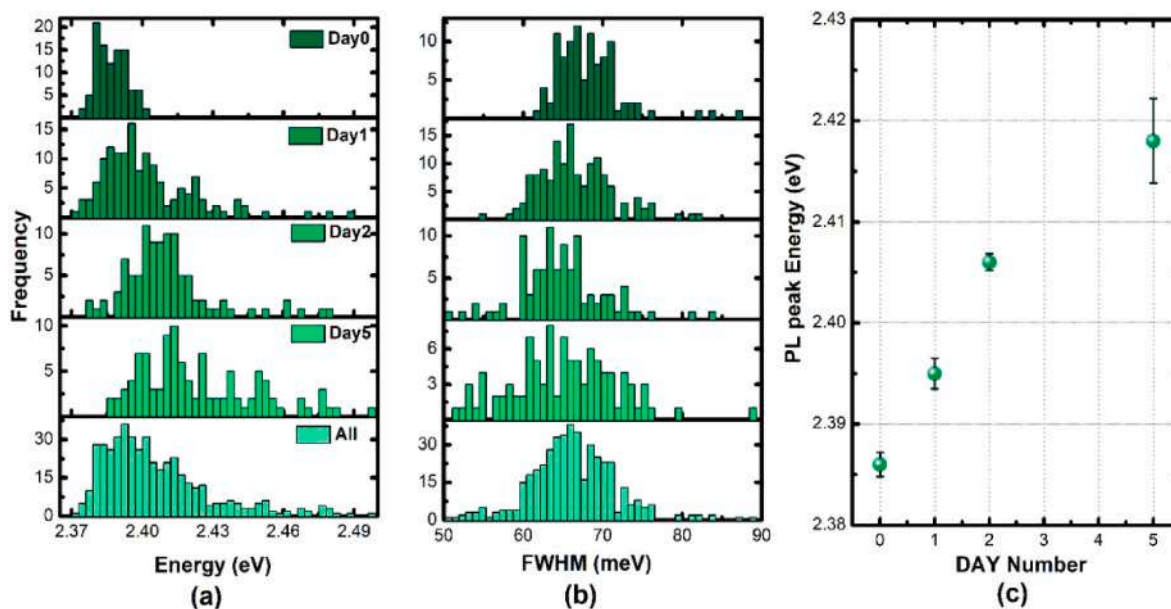
Fig. 5. Histograms regarding micro-PL statistics for peak energies (a) and FWHM (b), magnitudes that were extracted from micro-PL spectra measured at RT in around 100 CsPbBr$_3$ PNCs (from the second synthesis) of the same sample, but measured immediately after preparation (Day0), one (Day 1), two (Day 2) and five days after preparation (Day 5), respectively. (c) Dependence of the average micro-PL peak energy with aging time, as extracted from the frequency histograms in (a).

In the micro-PL statistics made on 100 CsPbBr$_3$ PNCs (Fig. 5) coming from the second synthesis (see section S1 for more details on the two synthetic routes), the average PL peak energy is around 2.386 eV immediately after its preparation (Day0 panel in Fig. 5a), smaller than in the case of the first synthesis (2.41 eV, see Fig. 4a), which is attributed to a larger average size of the PNCs (compare Figures S1b and S1d). Moreover, the observed dispersion in their micro-PL peak energies is approximately 20 meV, clearly smaller than their average homogeneous linewidth, 68 ± 4 meV (Day0 panel in Fig. 5b). The observed dispersion in PNCs from the second synthesis is clearly smaller than that exhibited in the case of the first synthesis (Fig. 4a), which is consistent with their significantly larger size distribution with a standard deviation of 2.3 nm (Figure S1b) as compared to the 0.8 nm value for the second synthesis (Figure S1d).

The analysis of the homogeneous linewidths extracted in single CsPbBr$_3$ PNCs (freshly samples) deserves special attention and further discussion. In the case of the second synthesis of PNCs, the data were highly concentrated around the average value of 68 ± 4 meV or 15.0 ±

1.5 nm (Day0 panel of Fig. 5b), whereas it is 94 ± 11 meV (20 ± 2 nm) in the case of CsPbBr$_3$ PNCs from the first synthesis. This difference could be tentatively ascribed to a higher sensitivity to ambient conditions of CsPbBr$_3$ PNCs obtained using the first synthesis. In fact, if one represents their FWHM versus micro-PL peak energies, a good linear correlation is obtained (Fig. 6a).

The homogeneous micro-PL linewidth of PNCs can be influenced by several physical mechanisms [35]:

(1) Fine structure of the excitonic fundamental state, which is related to crystal anisotropy or defect complexes in individual nanocrystals [36] and could be several meV. In our case, the contribution of biexcitons is discarded because the excitation power is quite low. This fine structure could be observed at low temperatures. In our samples, only single neutral exciton lines are measured under weak excitation power conditions (Fig. 3a–c).

(2) Spectral diffusion due to electric field fluctuations associated to dynamical charge surroundings. This mechanism would also be
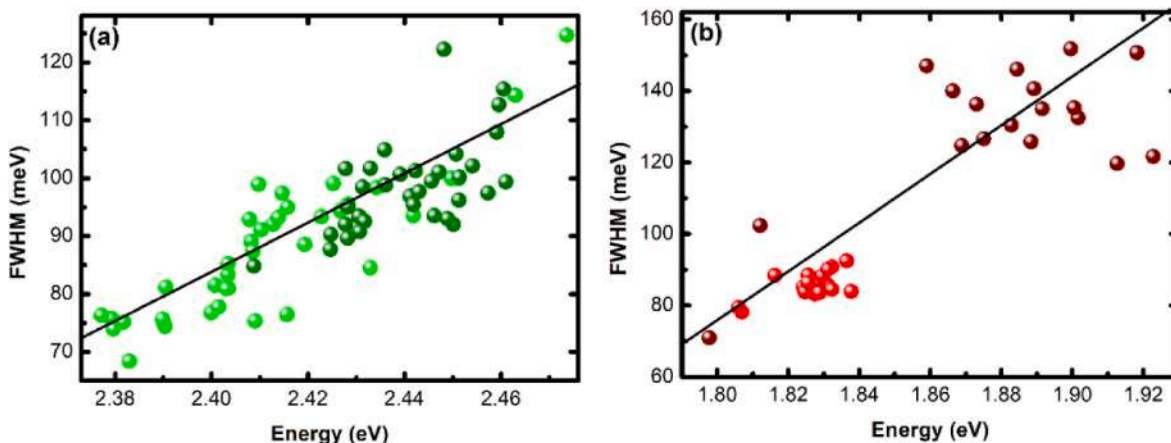

Fig. 6. Linear correlation between FWHM and peak energy extracted from its micro-PL spectrum in the 75 and 38 PNCs of CsPbBr$_3$ (a) and CsPbI$_3$ (b), respectively, studied in the present work. The experimental data points in light green and red (dark green and brown) correspond to the samples of CsPbBr$_3$ and CsPbI$_3$ measured immediately (next day) after preparation, respectively, together with the best fits to a straight line (black continuous line).

as large as several meV [36], depending on the charge environment and size [37]. In fact, we have measured linewidths from 1 (or slightly smaller) to 5 meV at 4 K in CsPbBr$_3$ PNCs (Figure S9a), whereas they are smaller than 0.5 meV in the case of CsPbI$_3$ (Figure S9b). In the present study, the spectral diffusion was more important in the first case, CsPbBr$_3$ PNCs, but it is highly dependent on the synthesis conditions and washing procedure.

(3) Exciton-phonon coupling would be negligible at 4 K, but its importance will increase by increasing temperature, due to the high coupling constant of excitons to polar optical phonons (Fröhlich interaction). This strong interaction was clearly demonstrated in studies of micro-PL on single PNCs of organo-halides FAPbBr$_3$ and FAPbI$_3$ (FA = Formamidinium) within the temperature range 4–150 K [38,39]. The exciton-phonon mechanism would give rise to a homogeneous linewidth of the excitonic optical transition in the order of 50 meV at RT for FAPbBr$_3$ and FAPbI$_3$ by extrapolating results reported in Refs. [38,39]. This estimate is not far from the lowest FWHM values measured in our PNCs of CsPbBr$_3$ (Fig. 5b, top panel), which means that the energy of the optical phonon and the exciton-phonon coupling constant will not differ significantly between both organic-inorganic and completely inorganic PNCs.

On the other hand, it is expected that the exciton-phonon coupling varies with the size of the PNC. This can be the reason of the approximate linear correlation between FWHM and peak energy extracted from the micro-PL spectra of fresh and one day old PNCs (Fig. 6). Theoretically, the PL peak energy will increase with size reduction (see section S3 in Supp. Info.). This linear correlation is also telling us that the exciton-phonon coupling constant would increase with the spatial quantum confinement in the nanocrystal, given that temperature is constant, and the phonon energy is not expected to vary until a very small nanocrystal size (several crystal unit cells).

Considering the observed linear correlation for CsPbBr$_3$ - CsPbI$_3$ PNCs in Fig. 6a–b, respectively, we can propose the following evolution for their Lorentzian homogeneous linewidth:

$$\Gamma_{NC} \cong \Gamma_{bulk} + \lambda\left[E_X^{NC} - E_X^{bulk}\right] \tag{1}$$

where Γ_{bulk} is the bulk exciton homogeneous linewidth, λ is the slope of the best fitting straight lines to experimental data (Fig. 6) and E_X^{NC}, E_X^{bulk} are the nanocrystal (introducing confinement) and bulk exciton energies, respectively. At RT we assume negligible the influence of other broadening mechanisms dependent on the nanocrystal size as discussed above (experimentally limited to several meV in Refs. [38,40] and our own results in Figure S9).

Equation (1) applied to experimental results in Fig. 6 would yield (assuming $E_X^{bulk} = 2.34$ eV [40] and $E_X^{bulk} = 1.746$ eV [41] for CsPbBr$_3$ and CsPbI$_3$, respectively):

$$\begin{cases} \Gamma_{NC} \cong 59 + 0.41\left[E_X^{NC} - 2340\right] meV & (CsPbBr_3) \\ \Gamma_{NC} \cong 40 + 0.677\left[E_X^{NC} - 1746\right] meV & (CsPbI_3) \end{cases} \tag{2}$$

The resulting value of $\Gamma_{bulk} \approx 59$ (40) meV for bulk CsPbBr$_3$ (CsPbI$_3$) is consistent with the expected value for the bulk exciton coupling with longitudinal optical (LO) phonons of energy $\hbar\omega_{LO} \approx 20$ (16) meV [40,42,43], excluded the effect of acoustic phonons that would be present in single crystals [42] and polycrystalline films of CsPbBr$_3$ (where other inhomogeneities could be also affecting the linewidth) [43], but not in PNCs [40]. On the other hand, the phonon-related linewidth of the light emission by a single PNC at 300 K would be directly proportional to the exciton-phonon coupling, $\gamma_{LO}^{NC}(E_X^{NC})$:

$$\Gamma_{NC} \cong \frac{\gamma_{LO}^{NC}\left(E_X^{NC}\right)}{e^{\frac{\hbar\omega_{LO}}{kT}} - 1} \tag{3}$$

Hence, from Equations (1)–(3), we would obtain:

$$\gamma_{LO}^{bulk} = \Gamma_{bulk}\left[e^{\frac{\hbar\omega_{LO}}{kT}} - 1\right] \approx 69\ (34) meV \quad CsPbBr_3(CsPbI_3) \tag{4}$$

$$\begin{cases} \gamma_{LO}^{NC}\left(E_X^{NC}\right) \cong 69 + 0.479\left[E_X^{NC} - 2340\right] meV & (CsPbBr_3) \\ \gamma_{LO}^{NC}\left(E_X^{NC}\right) \cong 34 + 0.580\left[E_X^{NC} - 1746\right] meV & (CsPbI_3) \end{cases} \tag{5}$$

The exciton-(LO) phonon coupling constant in bulk CsPbBr$_3$ and CsPbI$_3$ would be around 69 and 34 meV at RT, respectively, which are not far from values reported in Refs. [42,43], of course within the strong dispersion reported in literature (see Table S1 in Supp. Info.), as obtained from the application of the above given relations to our set of measurements in successive days (aging is giving rise to smaller size or higher PL peak energy). In fact, for CsPbBr$_3$ PNCs from our second synthesis, whose average peak energy was 2386 meV, we would expect a $\Gamma_{NC} \cong 78$ meV, around 15% higher than the deduced average value (68 meV). This relative difference is consistent with experimental error, shape fluctuations (cubic-parallelepipedal) and shape changes with the ambient influence along the duration of measurements, an influence which is especially important for PNCs grown following the first synthesis method (Fig. 6). In other words, if we take as more representative the average homogeneous linewidth of 68 meV for CsPbBr$_3$ PNCs, whose average edge size is 10.8 nm (Figure S1b), we would quantify the exciton-(LO) phonon coupling constant $\gamma_{LO}^{NC}(10.8\ nm) \approx 79$ meV at RT.

Another interesting aspect in the present study is the blue shift of the average micro-PL peak energy obtained from the statistical study of single nanocrystals at RT when the samples were measured the day after their preparation, as corroborated from histograms of Fig. 4b–d (in comparison to Fig. 4a–c) for CsPbBr$_3$–CsPbI$_3$ PNCs of the first synthesis and Fig. 5c for CsPbBr$_3$ PNCs of the second synthesis. In this latter case, the measured blue shift is around 10 meV/day, nearly a factor three smaller than the observed blue shift in CsPbBr$_3$ PNCs of the first synthesis. This conclusion points out towards a better stability of PNCs obtained by the modified method of synthesis in Ref. [44]. On the other hand, the PL blue shift effect could be attributed to deterioration against environmental conditions, as oxygen and humidity, mainly. The degradation effect in MAPbI$_3$ (MA = methylammonium) to environmental conditions is known [45,46], usually accompanied of a PL intensity decrease, more important under violet/ultraviolet laser excitation. At the level of individual PNCs, up to our knowledge there is only one study carried out on PNCs of CsPbI$_3$, in which a net blue shift of the micro-PL of PNCs was reported [47]. This study concluded that moisture could be the external agent with the greatest influence on PNCs, producing its gradual "dissolution", that is, a reduction of the PNC size over time. This possible size reduction effect would explain the observed energy blue shift, Δ, observed in our present work in one day, both in CsPbI$_3$ ($\Delta \approx 70$ meV) and CsPbBr$_3$ ($\Delta \approx 25$ meV) PNCs. Such PL peak energy blue shift does not alter our previous important observation regarding a low dispersion of peak energies as compared to the FWHM of micro-PL lines in single PNCs (Fig. 4).

These conclusions can be further understood by applying a quantum size confinement model that translates the nanocrystal size into its corresponding exciton energy (see Section S3 of the Supp. Info.). For PNCs of sizes larger than 8 nm the parabolic approximation (constant reduced exciton mass, μ') represented by Equation S6 is sufficiently good, as observed in Figure S10a. In this figure we compare the calculated values to several published data (also listed in Table S3). Moreover, a direct comparison can be made to our experimental micro-PL peak statistics by converting our size dispersion statistics (gaussian fit in Figure S1d for CsPbBr$_3$ PNCs of the second synthesis) into emission energy statistics, as made in Figure S10b under the parabolic (orange shaded curve) and nonparabolic (red shaded curve) approximations. Clearly, Equation S6 with constant μ' gives a shape as narrow as the experimental one, as given by the histogram of micro-PL energies (green bars in Figure S10b). This simple approximation is used in Fig. 7 to compare with experimental histograms (green bars) of micro-PL
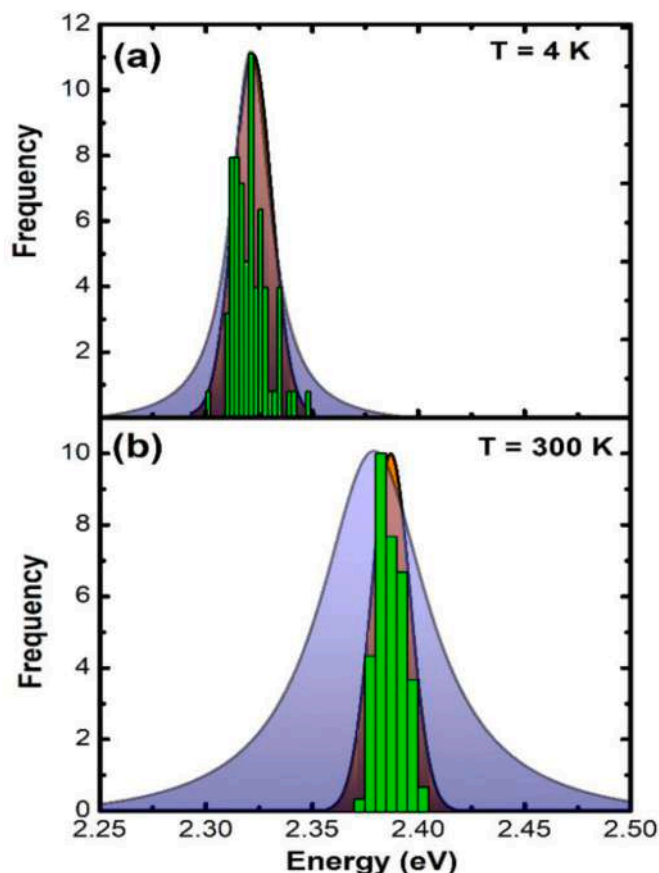
Fig. 7. Comparison of normalized PL spectra (shaded in blue) 4 K (a) and RT (b) for the high-density layer of CsPbBr$_3$ PNCs (second synthesis) as compared to the histograms (green bars) of micro-PL peak energies extracted from measurements in the sample just after preparation at 4 K (a) and RT (b) using the same CsPbBr$_3$ PNCs (second synthesis). Red shaded curves stand for the calculated (Equation S6) emission shape expected from the size histogram in these PNCs (Figure S1d).

energies measured for CsPbBr$_3$ PNCs (second synthesis) at 4 K (a) and RT (b). As anticipated above, the nanocrystal size distribution (Figure S1d) is the origin (red shaded curves) of the micro-PL energy dispersion (green bars) at both temperatures, which is below 30 meV, but only explains the inhomogeneously broadened PL of the high-density ensemble of PNCs at 4 K (blue shaded curve in Fig. 7a). This is not the case at RT, where the PL shape of the high-density sample (blue shaded curve in Fig. 7b) is clearly influenced by the large homogeneous linewidth due to exciton-phonon interaction, as previously discussed. It is worth noting the fact that the calculated shape at 4 K was done using an exciton energy for bulk of 2.289 eV, instead of 2.309 eV (see Table S2), even if this value was measured in a thin film [48]. More precise investigation on bulk CsPbBr$_3$ crystals would be needed to elucidate this discrepancy.

Finally, once validated the model for the estimation of exciton energies as a function of the cubic nanocrystal size, we can also corroborate that aging of single PNCs in ambient conditions is producing an effective reduction of their size. In fact, Figures S11-S12 demonstrate how aging in single CsPbBr$_3$ PNCs of the second synthesis (with a narrow size distribution) produce an effective reduction of their edge size by around 0.8 nm per day (for days 1 and 2), as observed in Figure S11 and S13a. In the case of PNCs from first synthesis the aging effect is more drastic, producing a size reduction of the order of 2.5 nm (see Figures S12 and S13b).

4. Conclusions

In this work, we have studied single CsPbBr$_3$ and CsPbI$_3$ PNCs by means of micro-PL spectroscopy. We have deduced average energies for the excitonic optical transitions of 2.414 and 1.83 eV for PNCs of CsPbBr$_3$ and CsPbI$_3$, respectively, in freshly prepared samples. In measurements taken after one day from the preparation of the samples, a blue shift of 25 and 70 meV was observed in the PL peak of CsPbBr$_3$ and CsPbI$_3$, respectively. This effect was explained by an effective reduction of the nanocrystal size in the order of the nm per day, probably due to the ambient humidity, as deduced by applying a cubic quantum dot model with finite potential barriers, which is also the base to obtain the expected peak energy dispersion (some tens of meV) from the PNC size distribution.

It is also noteworthy that for RT we have obtained the lowest values reported to date for the homogeneous micro-PL linewidth: 68 meV or 15 nm, in average, for isolated CsPbBr$_3$ PNCs. This value is characteristics of the exciton-phonon coupling interaction at RT in PNCs, whose constant γ_{LO} can be as large as 69 (34) meV for bulk CsPbBr$_3$ (CsPbI$_3$) and 79 meV for CsPbBr$_3$ PNCs with average edge size 10.8 nm. In the case of excitonic optical transitions at low temperatures (4 K), we have measured micro-PL linewidths in the range of 1–5 meV and 0.1–0.5 meV for CsPbBr$_3$ and CsPbI$_3$ PNCs, respectively. This indicates that CsPbBr$_3$ PNCs are more affected of spectral diffusion (internal electric field fluctuations). In any case, these linewidths are much smaller than the observed dispersion of micro-PL peak energy (inhomogeneous broadening expected in PNC ensembles), which is in the range of 30 meV, contrary to the case of RT, where the intrinsic exciton-phonon interaction is greater than the inhomogenous contribution produced by the size distribution. This effect allows to maintain the purity of color in dense layers of PNCs, of special relevance for applications to emitting devices.

Declaration of competing interest

The authors declare that they have no known competing financial interests or personal relationships that could have appeared to influence the work reported in this paper.

References

[1] Y.H. Kim, H. Cho, T.W. Lee, ''Metal halide perovskite light emitters, Proc. Natl. Acad. Sci. Unit. States Am. 113 (2016) 11694–11702, https://doi.org/10.1073/pnas.1607471113.
[2] Y.S. Park, S. Guo, N.S. Makarov, V.I. Klimov, Room temperature single-photon emission from individual perovskite quantum dots, ACS Nano 9 (2015) 10386–10393, https://doi.org/10.1021/acsnano.5b04584.
[3] U. Thumu, M. Piotrowski, B. Owens-Baird, Y.V. Kolen`ko, ''Zero-dimensional cesium lead halide perovskites: phase transformations, hybrid structures, and applications, J. Solid State Chem. 271 (2019) 361–377, https://doi.org/10.1016/j.jssc.2019.01.005.
[4] M. Ahmad, G. Rehman, L. Ali, M. Shafiq, R. Iqbal, R. Ahmad, T. Khan, S. Jalali-Asadabadi, M. Maqbool, I. Ahmad, ''Structural, electronic and optical properties of CsPbX3 (X= Cl, Br, I) for energy storage and hybrid solar cell applications, J. Alloys Compd. 705 (2017) 828–839, https://doi.org/10.1016/j.jallcom.2017.02.147.

[5] C. Huo, C.F. Fong, M.R. Amara, Y. Huang, B. Chen, H. Zhang, L. Guo, H. Li, W. Huang, C. Diederichs, Q. Xiong, Optical spectroscopy of single colloidal CsPbBr3 perovskite nanoplatelets, Nano Lett. 20 (2020) 3673–3680, https://doi.org/10.1021/acs.nanolett.0c00611.

[6] A.F. Gualdrón-Reyes, D.F. Macias-Pinilla, S. Masi, C. Echeverría-Arrondo, S. Agouram, V. Muñoz-Sanjosé, J. Rodríguez-Pereira, J.M. Macak, I. Mora-Seró, Engineering Sr-doping for enabling long-term stable FAPb1− xSrxI3 quantum dots with 100% photoluminescence quantum yield, J. Mater. Chem. C 9 (2021) 1555–1566, https://doi.org/10.1039/D0TC04625F.

[7] Y. Fu, H. Zhu, C.C. Stoumpos, Q. Ding, J. Wang, M.G. Kanatzidis, X. Zhu, S. Jin, Broad wavelength tunable robust lasing from single-crystal nanowires of cesium lead halide perovskites (CsPbX3, X= Cl, Br, I), ACS Nano 10 (2016) 7963–7972, https://doi.org/10.1021/acsnano.6b03916.

[8] M. Chen, Y. Zou, L. Wu, Q. Pan, D. Yang, H. Hu, Y. Tan, Q. Zhong, Y. Xu, H. Liu, B. Sun, Solvothermal synthesis of high-quality all-inorganic cesium lead halide perovskite nanocrystals: from nanocube to ultrathin nanowire, Adv. Funct. Mater. 27 (2017) 1701121, https://doi.org/10.1002/adfm.201701121.

[9] X. Li, Y. Wu, S. Zhang, B. Cai, Y. Gu, J. Song, H. Zeng, '' CsPbX3 quantum dots for lighting and displays: room-temperature synthesis, photoluminescence superiorities, underlying origins and white light-emitting diodes, Adv. Funct. Mater. 26 (2016) 2435–2445, https://doi.org/10.1002/adfm.201600109.

[10] A.B.F. Vitoreti, S. Agouram, M. Solis de la Fuente, V. Munoz-Sanjose, M.A. Schiavon, I. Mora-Seró, Study of the partial substitution of Pb by Sn in Cs–Pb–Sn–Br nanocrystals owing to obtaining stable nanoparticles with excellent optical properties, J. Phys. Chem. C 122 (2018) 14222–14231, https://doi.org/10.1021/acs.jpcc.8b02499.

[11] K.M. Salim, E. Hassanabadi, S. Masi, A.F. Gualdrón-Reyes, M. Franckevicius, A. Devizis, V. Gulbinas, A. Fakharuddin, I. Mora-Sero, Optimizing performance and operational stability of CsPbI3 quantum-dot-based light-emitting diodes by interface engineering, ACS Appl. Electron. Mater. 2 (2020) 2525–2534, https://doi.org/10.1021/acsaelm.0c00431.

[12] X. Lian, X. Wang, Y. Ling, E. Lochner, L. Tan, Y. Zhou, B. Ma, K. Hanson, H. Gao, Light emitting diodes based on inorganic composite halide perovskites, Adv. Funct. Mater. 29 (2019) 1807345, https://doi.org/10.1002/adfm.201807345.

[13] J. Navarro Arenas, A. Soosaimanickam, H. Pashaei Adl, R. Abargues, P. P Boix, P.J. Rodríguez-Cantó, J.P. Martínez-Pastor, Ligand-length modification in CsPbBr3 perovskite nanocrystals and bilayers with PbS quantum dots for improved photodetection performance, Nanomaterials 10 (2020) 1297, https://doi.org/10.3390/nano10071297.

[14] W. Zhang, X. Liu, B. He, Z. Gong, J. Zhu, Y. Ding, H. Chen, Q. Tang, Interface engineering of imidazolium ionic liquids toward efficient and stable CsPbBr3 perovskite solar cells, ACS Appl. Mater. Interfaces 12 (2020) 4540–4548, https://doi.org/10.1021/acsami.9b02831.

[15] E.A. Erazo, H.E. Sánchez-Godoy, A.F. Gualdrón-Reyes, S. Masi, I. Mora-Seró, Photo-Induced black phase stabilization of CsPbI3 QDs films, Nanomaterials 10 (2020) 1586, https://doi.org/10.3390/nano10081586.

[16] M. Hao, Y. Bai, S. Zeiske, L. Ren, J. Liu, Y. Yuan, N. Zarrabi, N. Cheng, M. Ghasemi, P. Chen, M. Lyu, Ligand-assisted cation-exchange engineering for high-efficiency colloidal Cs1−xFAxPbI3 quantum dot solar cells with reduced phase segregation, Nat. Energy 5 (2020) 79–88, https://doi.org/10.1038/s41560-019-0535-7.

[17] A. Swarnkar, A.R. Marshall, E.M. Sanehira, B.D. Chernomordik, D.T. Moore, J.A. Christians, T. Chakrabarti, J.M. Luther, Quantum dot–induced phase stabilization of α-CsPbI3 perovskite for high-efficiency photovoltaics, Science 354 (2016) 92–95, https://doi.org/10.1126/science.aag2700.

[18] NREL, Best Research-Cell Efficiency Chart, 2021. https://www.nrel.gov/pv/cell-efficiency.html.

[19] M.C. Brennan, M. Kuno, S. Rouvimov, Crystal structure of individual CsPbBr3 perovskite nanocubes, Inorg. Chem. 58 (2019) 1555–1560, https://doi.org/10.1021/acs.inorgchem.8b03078.

[20] A.F. Gualdrón-Reyes, S. Masi, I. Mora-Seró, Progress in halide-perovskite nanocrystals with near-unity photoluminescence quantum yield, Trends Chem 3 (2021) 499–511, https://doi.org/10.1016/j.trechm.2021.03.005.

[21] Y. Fu, X. He, J. Hu, Y. Zhang, N. Lian, Z. Li, Y. Zhou, Comparison of superstar CsPbBr3 and classical LaPO4: Tb3+, Ce3+ green-emitting nanophosphors, Mater. Res. Express 6 (2018) 055017, https://doi.org/10.1088/2053-1591/ab0165.

[22] J. Pan, Y. Shang, J. Yin, M. De Bastiani, W. Peng, I. Dursun, L. Sinatra, A.M. El-Zohry, M.N. Hedhili, A.H. Emwas, O.F. Mohammed, Bidentate ligand-passivated CsPbI3 perovskite nanocrystals for stable near-unity photoluminescence quantum yield and efficient red light-emitting diodes, JACS 140 (2018) 562–565, https://doi.org/10.1021/jacs.7b10647.

[23] N. Mondal, A. De, A. Samanta, Achieving near-unity photoluminiscence efficiency for blue-violet-emitting perovskite nanocrystals, ACS Energy Lett 4 (2019) 32–39, https://doi.org/10.1021/acsenergylett.8b01909.

[24] I. Suárez, T. Wood, J.P.M. Pastor, D. Balestri, S. Checcucci, T. David, M. Gurioli, Enhanced nanoscopy of individual CsPbBr3 perovskite nanocrystals using dielectric sub-micrometric antennas, Apl. Mater. 8 (2020), 021109, https://doi.org/10.1063/1.5142225.

[25] H.P. Adl, S. Gorji, M.K. Habil, I. Suárez, V.S. Chirvony, A.F. Gualdrón-Reyes, J.P. Martínez-Pastor, Purcell enhancement and wavelength shift of emitted light by CsPbI3 perovskite nanocrystals coupled to hyperbolic metamaterials, ACS Photonics 7 (2020) 3152–3160, https://doi.org/10.1021/acsphotonics.0c01219.

[26] J.P. Martinez-Pastor, H.P. Adl, S. Gorji, J. Navarro-Arenas, G. Muñoz-Matutano, I. Suárez, V.S. Chirvony, A.F. Gualdrón-Reyes, I. Mora-Seró, Lead halide perovskite nanocrystals: optical properties and nanophotonics, Proc. SPIE 11800 (2021), https://doi.org/10.1117/12.2595442. Low-Dimensional Materials and Devices, 1180013.

[27] J. Navarro-Arenas, I. Suárez, V.S. Chirvony, A.F. Gualdrón-Reyes, I. Mora-Seró, J. Martínez-Pastor, Single-exciton amplified spontaneous emission in thin films of CsPbX3 (X= Br, I) perovskite nanocrystals, J. Phys. Chem. Lett. 10 (2019) 6389–6398, https://doi.org/10.1021/acs.jpclett.9b02369.

[28] F. Hu, H. Zhang, C. Sun, C. Yin, B. Lv, C. Zhang, W.W. Yu, X. Wang, Y. Zhang, M. Xiao, Single photon emission from single perovskite nanocrystals of cesium lead bromide, ACS Nano 9 (2015) 12410–12416, https://doi.org/10.1021/acsnano.5b05769.

[29] H. Utzat, W. Sun, A.E. Kaplan, F. Krieg, M. Ginterseder, B. Spokoyny, N.D. Klein, K.E. Shulenberger, C.F. Perkinson, M.V. Kovalenko, M.G. Bawendi, Coherent single-photon emission from colloidal lead halide perovskite quantum dots, Science 363 (2019) 1068–1072, https://doi.org/10.1126/science.aau7392.

[30] G. Rainò, A. Landuyt, F. Krieg, C. Bernasconi, S.T. Ochsenbein, D.N. Dirin, M.I. Bodnarchuk, M.V. Kovalenko, Underestimated effect of a polymer matrix on the light emission of single CsPbBr3 nanocrystals, Nano Lett. 19 (2019) 3648–3653, https://doi.org/10.1021/acs.nanolett.9b00689.

[31] L. Protesescu, S. Yakunin, M.I. Bodnarchuk, F. Krieg, R. Caputo, C.H. Hendon, R.X. Yang, A. Walsh, M.V. Kovalenko, Nanocrystals of cesium lead halide perovskites (CsPbX3, X = Cl, Br, and I): novel optoelectronic materials showing bright emission with wide color gamut, Nano Lett. 15 (2015) 3692–3696, https://doi.org/10.1021/nl5048779.

[32] I. Suarez, M. Vallés-Pelarda, A.F. Gualdrón-Reyes, I. Mora-Sero, A. Ferrando, H. Michinel, J. R y Salgueiro, J.P. Martinez-Pastor, "Outstanding nonlinear optical properties of methylammonium- and Cs-PbX 3 (X = Br, I, and Br–I) perovskites: polycrystalline thin films and nanoparticles", Apl. Mater. 7 (2019), 041106 https://doi.org/10.1063/1.5090926.

[33] S. Masi, A.F. Gualdrón-Reyes, I. Mora-Sero, Stabilization of black perovskite phase in FAPbI3 and CsPbI3, ACS Energy Lett 5 (2020) 1974–1985, https://doi.org/10.1021/acsenergylett.0c00801.

[34] H.C. Yoon, H. Kang, S. Lee, J.H. Oh, H. Yang, Y.R. y Do, Study of perovskite QD down-converted LEDs and six-color white LEDs for future displays with excellent color performance, ACS Appl. Mater. Interfaces 8 (2016) 18189–18200, https://doi.org/10.1021/acsami.6b05468.

[35] T.G. Mack, L. Jethi, P. y Kambhampati, Temperature dependence of emission line widths from semiconductor nanocrystals reveals vibronic contributions to line broadening processes, J. Phys. Chem. C 121 (2017) 28537–28545, https://doi.org/10.1021/acs.jpcc.7b09903.

[36] G. Rainò, G. Nedelcu, L. Protesescu, M.I. Bodnarchuk, M.V. Kovalenko, R.F. Mahrt, T. Stoferle, Single cesium lead halide perovskite nanocrystals at low temperature: fast single-photon emission, reduced blinking, and exciton fine structure, ACS Nano 10 (2018) 2485–2490, https://doi.org/10.1021/acsnano.5b07328.

[37] C. Heyn, L. Ranasinghe, M. Zocher, W. Hansen, Shape-dependent Stark shift and emission-line broadening of quantum dots and rings, J. Phys. Chem. C 124 (2020) 19809–19816, https://doi.org/10.1021/acs.jpcc.0c05043.

[38] O. Pfingsten, J. Klein, L. Protesescu, M.I. Bodnarchuk, M.V. Kovalenko, G. Bacher, Phonon interaction and phase transition in single Formamidinium lead bromide quantum dots, Nano Lett. 18 (2018) 4440–4446, https://doi.org/10.1021/acs.nanolett.8b01523.

[39] M. Fu, P. Tamarat, J.B. Trebbia, M.I. Bodnarchuk, M.V. Kovalenko, J. Even, B. Lounis, Unraveling exciton–phonon coupling in individual FAPbI3 nanocrystals emitting near-infrared single photons, Nat. Commun. 9 (2018) 3318, https://doi.org/10.1038/s41467-018-05876-0.

[40] C.M. Iaru, J.J. Geuchies, P.M. Koenraad, D. Vanmaekelbergh, A.Y. Silov, Strong Carrier−Phonon coupling in lead halide perovskite nanocrystals, ACS Nano 11 (2017) 11024–11030, https://doi.org/10.1021/acsnano.7b05033.

[41] C.C. Stoumpos, C.D. Malliakas, M.G. Kanatzidis, Semiconducting tin and lead iodide perovskites with organic cations: phase transitions, high mobilities, and near-infrared photoluminescent properties, Inorg. Chem. 52 (2013) 9019–9038, https://doi.org/10.1021/ic401215x.

[42] M. Nagai, T. Tomioka, M. Ashida, M. Hoyano, R. Akashi, Y. Yamada, T. Aharen, Y. Kanemitsu, Longitudinal optical phonons modified by organic molecular cation motions in organic-inorganic hybrid perovskites, Phys. Rev. Lett. 121 (2018) 145506, https://doi.org/10.1103/PhysRevLett.121.145506.

[43] C. Wolf, T.W. Lee, Exciton and lattice dynamics in low-temperature processable CsPbBr3 thin-films, Mater. Today Energy 7 (2018) 199–207, https://doi.org/10.1016/j.mtener.2017.09.010.

[44] A.F. Gualdron-Reyes, S.J. Yoon, E.M. Barea, S. Agouram, V. Munoz-Sanjose, A.M. Melendez, M.E. Nino-Gomez, I. Mora-Sero, Controlling the phase segregation in mixed halide perovskites through nanocrystal size, ACS Energy Lett 4 (2019) 54–62, https://doi.org/10.1021/acsenergylett.8b02207.

[45] Y. Ouyang, L. Shi, Q. Li, J. Wang, Role of water and defects in photo-oxidative degradation of methylammonium lead iodide perovskite, Small Methods 3 (2019) 1900154, https://doi.org/10.1002/smtd.201900154.

[46] M. Anaya, J.F. Galisteo-López, M.E. Calvo, J.P. Espinós, H. Míguez, Origin of light-induced photophysical effects in organic metal halide perovskites in the presence of oxygen, J. Phys. Chem. Lett. 9 (2018) 3891–3896, https://doi.org/10.1021/acs.jpclett.8b01830.

[47] G. Yuan, C. Ritchie, M. Ritter, S. Murphy, D.E. Gómez, P. y Mulvaney, The degradation and blinking of single CsPbI3 perovskite quantum dots, J. Phys. Chem. C 122 (2018) 13407–13415, https://doi.org/10.1021/acs.jpcc.7b11168.

[48] Z. Yang, A. Surrente, K. Galkowski, A. Miyata, O. Portugall, R.J. Sutton, A.A. Haghighirad, H.J. Snaith, D.K. Maude, P. Plochocka, R.J. Nicholas, Impact of the halide cage on the electronic properties of fully inorganic cesium lead halide perovskites, ACS Energy Lett 2 (2017) 1621–1627, https://doi.org/10.1021/acsenergylett.7b00416.